The 10 micron instrument MIDI – getting ready for observations on the VLTI

Christoph Leinert[a] and Uwe Graser[a];
Laurens B.F.M. Waters[b]; Guy Perrin[c]; Walter Jaffe[d], Bruno Lopez[e];
Frank Przygodda[a], Olivier Chesneau[a], Peter Schuller[a], Annelie Glazenborg-Kluttig[f],
Bernhard Grimm[a], Werner Laun[a], Sebastiano Ligori[a], Jeff Meisner[d], Karl Wagner[a];
Eric Bakker[d], Bill Cotton[g], Jeroen de Jong[d], Richard Mathar[a], Udo Neumann[a], Clemens Storz[a]

[a]Max-Planck-Institut für Astronomie, Heidelberg, Germany
[b]Astronomical Institute, University of Amsterdam, Netherlands
[c]DESPA, Observatoire de Paris-Meudon, France
[d]Sterrewacht Leiden, University of Leiden, Netherlands
[e]Observatoire de la Côte d'Azur, Nice, France
[f]ASTRON, Dwingeloo, Netherlands
[g]NRAO, Charlottesville, Virginia, USA

ABSTRACT

The mid-infrared interferometric instrument MIDI is currently undergoing testing in preparation for commissioning on the Very Large Telescope Interferometer VLTI at the end of this year 2002. It will perform interferometric observations over the 8 μm - 13 μm wavelength range, with a spatial resolution of 20 milliarcsec, a spectral resolution of up to 250, and an anticipated point source sensitivity of N = 4 mag or 1 Jy for self - fringe tracking, which will be the only observing mode during the first months of operation. We describe the layout of the instrument and the performance during laboratory tests, both for broadband and spectrally resolved observing modes. We also briefly outline the planned guaranteed time observations.

Keywords: Interferometry, interferometric instrument, mid-infrared, VLTI, MIDI

1. INTRODUCTION

The mid-infrared interferometric instrument MIDI, covering the full 8 μm - 13 μm range of the N band, is one of the two first generation instruments of the Very Large Telescope Interferometer (VLTI), the second one, AMBER, working in the near-infrared. After successful commissioning MIDI will be the first instrument doing direct combination 10 μm interferometry worldwide. Its main advantage with respect to the quite successful ISI heterodyne interferometer (Bester et al.[1]) will be higher sensitivity, due both to the larger diameter telescopes of the VLTI and the ability for broadband operation with MIDI.

2. PRINCIPLE

Conceptual design started in 1997. A schematic representation of the layout of the instrument is given in Figure 1.

Since radiation at 10 μm is dominated by thermal emission from the environment, most of the instruments optics has to be in a dewar and to be cooled to cryogenic temperatures (5 K - 10 K for the detector, 40±5 K for the cold bench, 77 K for the outer radiation shield). Good suppression of the thermal radiation of background and surroundings requires to design for both a cold pupil and a cold field stop inside the instrument. We choose

Send correspondence to: Christoph Leinert, Max-Planck-Institut für Astronomie, Königstuhl 17, D-69117 Heidelberg, Germany; e-mail: leinert@mpia-hd.mpg.de

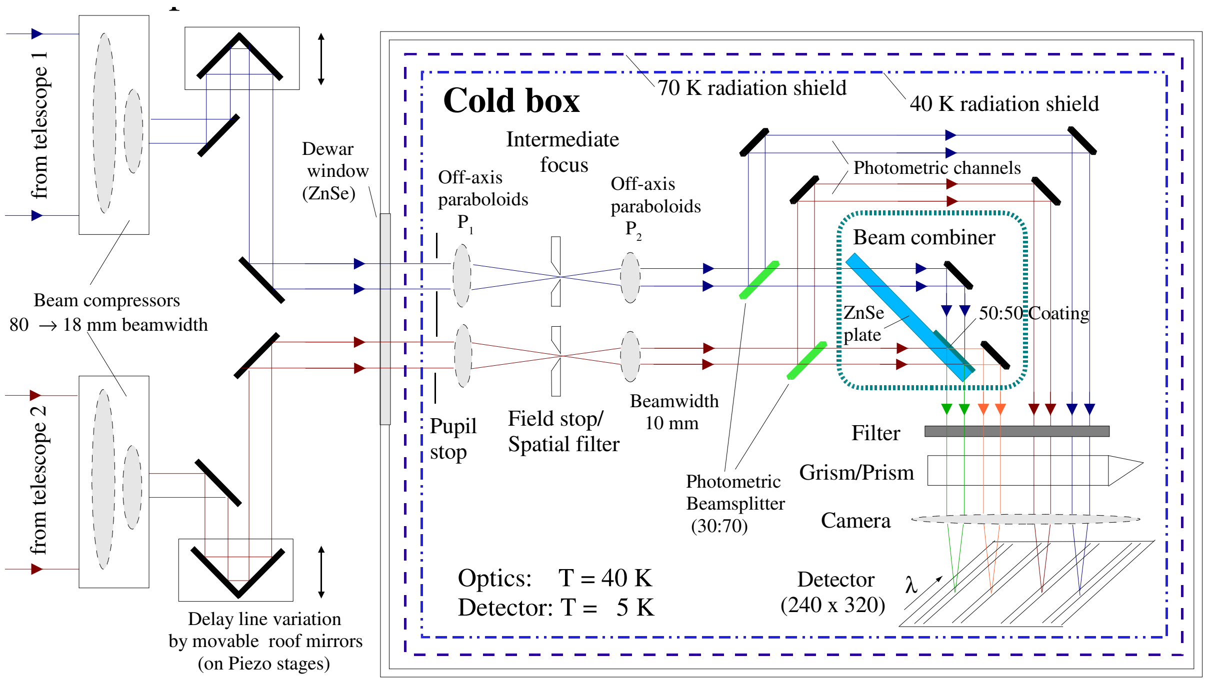

Figure 1. Schematic diagram of the instrument

to have beam combination in (or close to) the pupil and to detect the signal in the image plane. This appeared to us the most promising way to support the baffling against the very high thermal background and to reduce the effects of variable pixel responsivity.

This leads to the following optical concept: from the left, the afocal beams from two telescopes of the VLTI are approaching the instrument. Their nominal diameter is 80 mm, and they are reduced to 18 mm diameter by a beam compressor provided as part of the VLTI infrastructure, represented here for simplicity by two lenses.

After the four folding mirrors of a small experiment-internal delay line, the compressed beams enter the cryostat ("Cold box") through the entrance window ("Dewar window"). The telescope pupil is imaged by the VLTI delay line optics onto a cold pupil stop to provide the needed suppression of thermal emission from outside the beams. Next, an intermediate focus is formed, where different slits or diaphragms (i.e. spatial filters) can be introduced for additional suppression of unwanted radiation. If no spatial filters are used, the detector pixels, which are much smaller than the Airy disk, still provide an alternative way to limit the spatial region admitted for the measurement. Then the beams are recollimated (again, reflective optics is represented by a lens for simplicity) and move on to combine on the surface of a 50%:50% beam splitter. This coating is indicated in the Figure on the lower back side of the ZnSe plate. This is the heart of the instrument.

From the beam combiner onwards, the two interfering beams have a common optical axis. Actually, there are two of such overlaid beams, one outgoing to each side of the beam combiner. These two outputs are modulated in flux depending on the optical path difference of the interfering beams, but with opposite sense because of energy conservation.

We measure the degree of coherence between the interfering beams (i.e. the object visibility at the actual baseline setting) by artificially stepping the optical path difference between the two input beams rapidly over at least one wavelength within the coherence time of ≈ 0.1 s. This is done with help of the piezo-driven roof mirrors forming part of the small delay lines just outside the cryostat. The result in both channels is a signal modulated with time ("temporal fringe"), from which the fringe amplitude can be determined. The large and not precisely known thermal background forces us to determine the total flux separately by a chopped measurement, chopping

Figure 2. The MIDI instrument in the laboratory in nominal setup. The dewar sits on its table with the warm optics bench in front of it. In the background the calibration unit table can be seen at right as well as two of the three electronic cabinets. These other units will be not in the interferometric laboratory but in the adjacent room. On the warm optics bench, the telescopes used for alignment can be seen at left, the black shoe-sized box in the middle carries a black screen filling the field-of-view for defined stimulation of the instrument.

between the object and an empty region of the sky, and determining the source flux by subtraction. Dividing fringe amplitude by total flux the visibility is obtained.

If the flux is not the same in the two incoming beams, the visibility gets reduced by the ratio of geometrical to arithmetic mean of the two fluxes. Therefore, for good accuracy of the visibility determination, the relative fluxes of the combining beams have to be known at the time of the fringe measurement. To this end, part of the incoming light can be extracted out of both of the incoming beams before beam combination, and these so-called 'photometric beams' or 'photometric channels' are also imaged onto the same detector and in the same way as the interferometric signal.

Spectral resolution is obtained by filters or with a prism or grism in the parallel beam after beam combination. This provides moderate spectral resolution and at the same time keeps the detector from saturating within the order of 1 ms.

In principle, for the measurements with MIDI the full interferometric field of $\pm 1''$ is available simultaneously. This is a small area on the sky, but about 8 times larger than the FWHM of the Airy disk of a single telescope, to which interferometric measurements are normally limited.

For later reference we mention that the upper uncoming beam in Figure 1 is called "A", the lower one "B", the associated extracted photometric channels are called "P_A" and "P_B", the interformetric channels "I_1" and "I_2", where I_1 corresponds to the transmitted continuation of beam A, leftmost on the detector in the schematic diagram of Figure 1. The actual design and realization of the instrument optics is described elsewhere in these proceedings (Glazenborg-Kluttig et al.[2]).

3. STATUS

MIDI now is fully assembled in a laboratory at the Max-Planck-Institut für Astronomie (MPIA) in Heidelberg and undergoing extensive testing. Figure 2 shows the integrated instrument and its main functional parts: (1) dewar with cold optics on a big optical table, (2) warm optics for adapting to the incoming beams from the VLTI and for input of light from a laboratory light source for testing, all of this on an optical bench on top of the big table, (3) a separated table for the laboratory light source. The cabinets next to this table contain the control electronics as well as the read-out electronics for the detector – a major in-house development. Figure 3 gives an impression of the dimensions of the instrument.

Figure 3. Assembly of the MIDI dewar by Werner Morr (left) and Armin Böhm. What looks like a four storage building is the 77 K shield with the liquid nitrogen tank on top.

The **cold optics** with a few baffles and the detector housing taken out is shown in Figure 4. In spite of the crowded design, care has been taken to have all subunits removable from top. The alignment procedure, straightforward once established but not short and not easy to design, also is described in [2]. Alignment is done in the warm and checked in the cold. The goal of having no measurable change of alignment between warm and cold has been almost reached, to less than one pixel when using the longer focal length field camera.

A functional diagram of the **warm optics** is shown in Figure 5 with the optics put into position to allow the measurement of the internal laser source. Then the beams coming from the VLTI are exchanged for the two laser beams created by a beamsplitter on the warm optics. Note the three positions to put alignment plates: for alignment towards the cold optics (top), for alignment towards the VLTI (bottom) and for alignment towards the laser calibration source (right). Figure 6 shows the actual hardware of the warm optics. To keep the piezo response fast, the roof mirrors mounted on top of them (one seen at upper middle left of the Figure) were manufactured from beryllium, with a resulting mass including mounting and screws of less than 19 g.

The **table for the laboratory light sources** carries a CO_2 laser radiating at 10.6 μm with suitable attenuating to bring it to the brightness range observable by MIDI. It provides an absolute wavelength reference and input beams corresponding to a high visibility (almost unresolved) source. For laboratory tests as long as the 10 μm calibration sources of the VLTI will not be available, in addition light from a blackbody source can be injected by the usual way: producing afocal beams of a point-like source by illuminating a pinhole in the focus of a paraboloid.

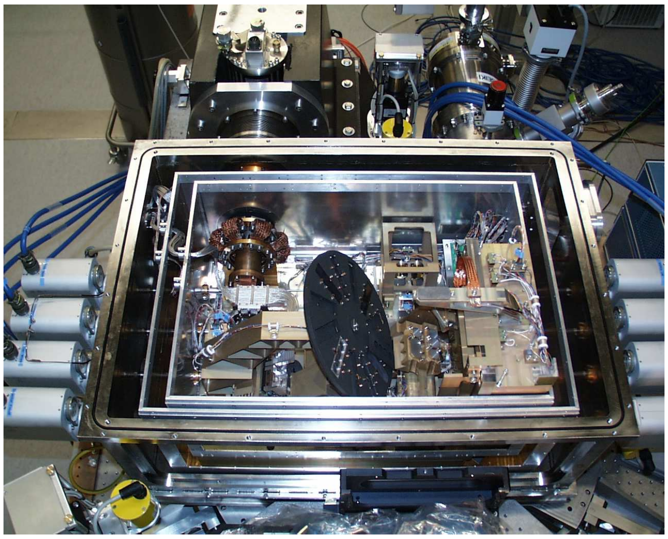

Figure 4. View on the cold optics inside the opened dewar. Clearly seen are the blackened filter wheel slightly left of the middle and cold head on the upper left, with its cylindrical cold "finger" penetrating into the area of the cold optics. On the left and right wall of the dewar each carry four encapsulated motor/encoder units, which drive the mechanisms of the cold optics with axes pentrating the wall of the dewar and the two radiation shields.

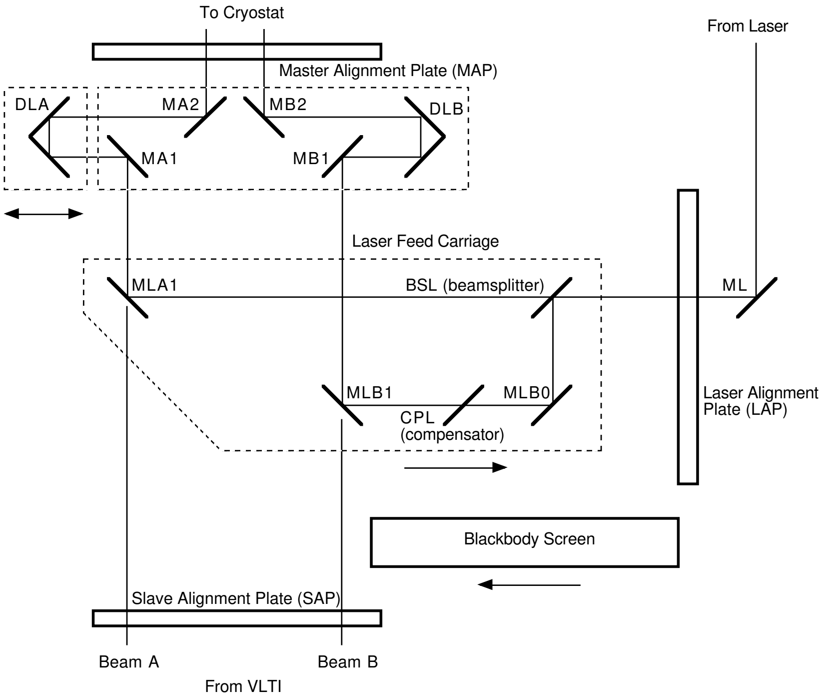

Figure 5. Functional diagram of the warm optics.

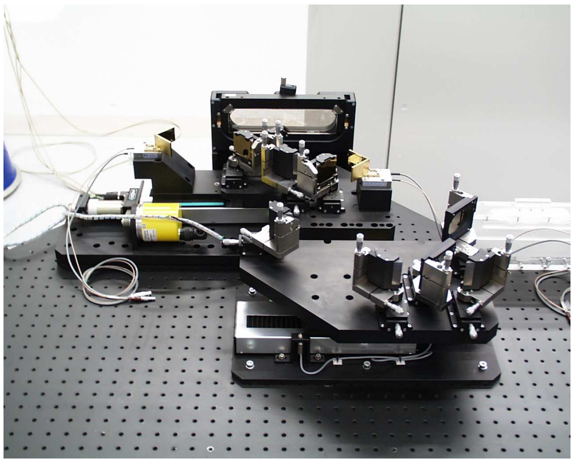

Figure 6. Main parts of the warm optics of MIDI. The folding mirrors adapting the beam separation and providing path difference modulation are shown (middle grouping) as well as the sliding table for calibration laser input (in front) and the master alignment plate in its elongated mount on the far side of the folding mirrors.

4. CHOICES IN THE OPTICAL SETUP

The instrument provides flexibility by several choices in the optical setup, which are summarised in the following tabular presentation. Not all combinations are equally meaningful: grism and prism normally should be used with the spectral camera, filters with the field camera, while the pupil camera is for testing purposes. One pixel on the detector is 50 μm in size, λ/D for 10 μm and 8 m telescope diameter corresponds to 0.258″ on the sky.

cameras	field camera	λ/D = 3 pixels
	spectal camera	λ/D = 1x2 pixels (1 in spectral, 2 in spatial direction)
	pupil viewing camera	pupil diameter = 40 pixels
dispersing elements	grism	resolution per two pixels = 220 at 10 μm
	prism	resolution per two pixels = 35 at 10 μm
	none	for observations with filters
filters	10 filters	in cluding full N-band, short N (8.0 - 9.5 μm), long N (10.5 - 13.1 μm), narrow bands, neutral density 1.0
focal plane	no diaphragm	2 mm diameter (overfilling the VLTI beam)
	full interferometric field	1 mm diameter (± 1.3″ on UTs)
	slits (1 mm long)	50 μm, 100 μm, 200 μm, (0.5 - 2 λ/D)
	single pinhole	0.4 mm diameter, (1.0″ on UTs)
	triple pinholes – spaced at 0.29 mm	70 μm, 110 μm, 170 μm (0.7 - 1.7 λ/D) (diameter)
beamcombiner unit	high sensitivity	no photometric beam extraction
	with photometric beams	30 % of light in photometric channels
	open	no beam combination

In addition, special setups are available for testing and alignment. The mechanical spaces for future 20 μm optical components already are provided, allowing an easy upgrade to this second wavelength range.

5. MEASURING MODES - LABORATOY TESTS

The **detector** is a Si:As impurity band conduction (IBC) array produced by Raethyon, 320x240 pixels in size. It is read out in 16 bands, each 20 pixels wide, which gives rise to the band structure seen, e.g., in Figure 7, right panel. The readout noise is $\approx$ 1000 electrons. The readout electronics, quite flexible, allows a full frame readout time of 5.6 ms, which time can be further reduced by reading only rows of relevance for the current observation (so-called "hardware windowing"). Integration time is not influenced by readout time. Standard operation is first to take the exposure, then to read out ("integrate then read"). More details are given in [3]. In the following pictures the detector is always shown as seen with incoming light.

Figure 7 shows how in **undispersed** mode data will typically be arranged on the detector. Using a slit, the appearance will be similar like for the triple pinholes, but with about 50 % larger extension along the y axis. Figure 8 shows corresponding patterns for measurements in **dispersed** mode.

Figure 7. Images on the detector (320x240 pixels) when using the field camera and no dispersive device. The leftmost 80 pixel rows are omitted. *Left*: Focal plane diaphragm fully open. The interferometric beams I_2 (up) and I_1 (low) are shown. The 5″ diameter field (for UT plate scale) is filled by background radiation. Above the center a test point source can be seen. The rest of the detector area is unexposed. *Middle*: Same, but with a triple pinhole illuminated by background radiation. *Right*: With photometric beams extracted, P_A (top) and P_B (bottom) now appear in addition.

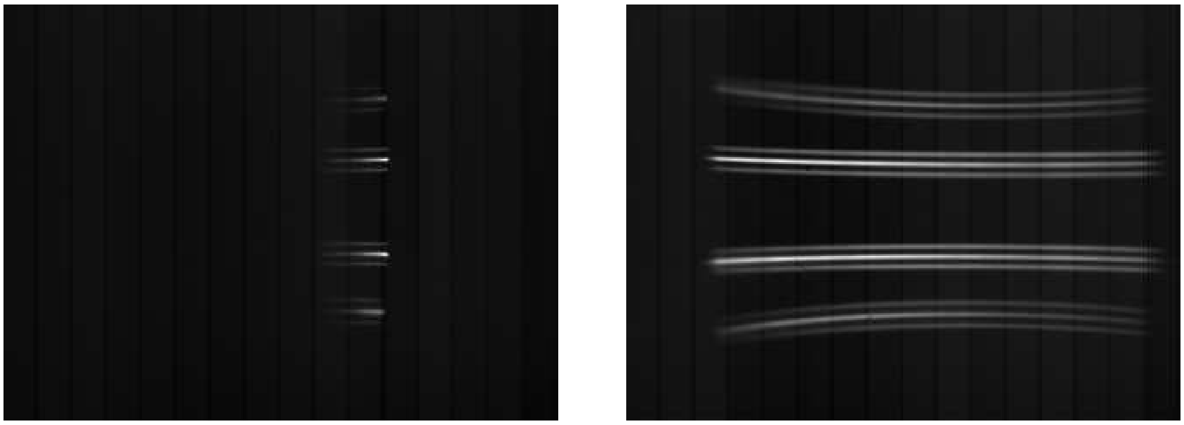

Figure 8. Images on the detector (320x240 pixels) when using a dispersive device and the spectral camera. Triple pinholes are selected for focal diaphragm and photometric beam extraction is performed. The light of a test point source is fed into the central one of the pinhole triple. *Left*: Typical exposure with prism. From top to bottom the channels P_A, I_2, I_1, P_B are shown. Short wavelengths are at right, long wavelengths at left. *Right*: Typical exposure with the grism in place. Here, short wavelength (8 μm) are at left, long wavelengths (13 μm) are at right.

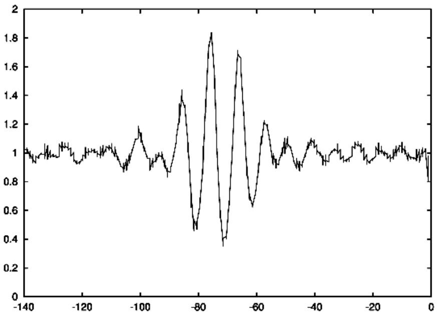

Figure 9. Fringes measured in the laboratory in one of the interferometric channels in undispersed mod. The fringe packet appears as temporal modulation when scanning the OPD by means of one of the piezo-mounted mirrors. The signal is normalised to the average, the relative optical path difference is given in μm.

A natural way of interferometric observations with an on-axis combining instrument like MIDI is to measure the fringe amplitude from the temporal modulation of the signal obtained when **scanning** the OPD by means of the instrument-internal piezo drivers. Figure 9 shows such a scan taken with the full N band filter. After determination of the background level, a measured raw visibility of 80 % was deduced. This sets an upper limit for the instrumental loss of visibility inside MIDI to 20 %. In Figure 9, zero OPD occurs at a scan position of about -72 μm. The interference pattern is similar to a damped sine wave around this origin. This is the expected behaviour for combination on a beam splitting surface. It is not a design suited for interferometric nulling because in broadband observations it will lead to damping already in the first maximum.

Alternatively, the fringe amplitude can be determined in **dispersed** data from the modulation along the

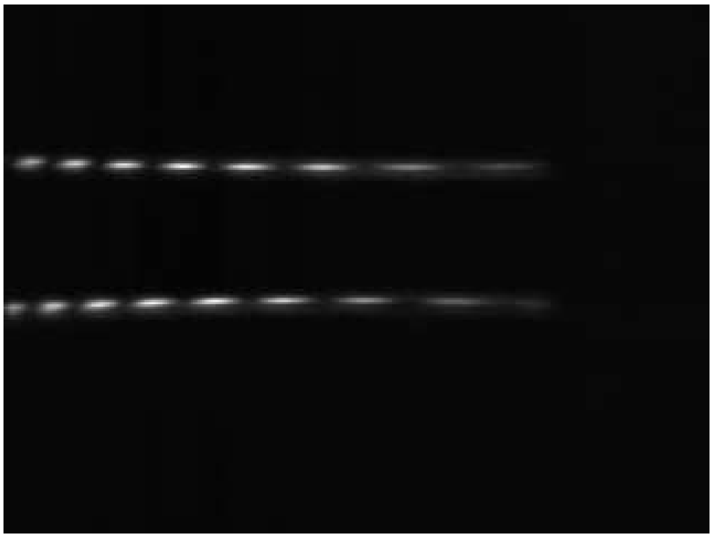

Figure 10. Dispersed fringes measured in the laboratory. Basically, one exposure giving the output of channels I_2 (up) and I_1 (down) is shown. The instrument setup corresponds to the left of Figure 7, and background has been subtracted. Note the opposite phase of constructive and destructive interference in the two channels, as well as the modulation with wavelength with frequency $1/\lambda$, which makes the pattern more closely spaced at the left, short wavelength end. Offset from zero OPD is about 140 μm

spectrum ("channeled spectrum") occuring when the OPD is offset from zero (Figure 10). Although the coherence length is hundreds of microns for each spectral element in this case, short exposures have to be taken nevertheless. Otherwise the fringe motion resulting from atmospheric turbulence would smear out the modulation. As already mentioned, in both cases photometry – usually by chopping – is needed in addition to derive the source visibility.

Self-fringe-tracking in the undispersed mode tries to keep the fringe packet centered in the – usually quite a bit shorter than shown in Figure 9 – scan window. Self-fringe-tracking in dispersed mode tries to keep the OPD offset from zero at the same, constant value.

6. BASIC PARAMETERS AND EXPECTED PERFORMANCE

Most of the parameters defining the operation of the instrument are given by the atmosphere or the VLTI. However, the choice to observe only one baseline at a time was made to keep sensitivity.

Telescope diameter	UTs	8 m
	ATs	1.8 m (used for bright sources)
Baselines available	UTs	47 ... 130 m
– only one at a time	ATs	8 ... 200 m
Resolution	λ / D for 100 m	0.020″ at 10 μm
Wavelength coverage		N band (8 μm - 13 μm)
	expandable to	Q band (17 μ - 26 μm)
Interferometric field of view	UTs	$\pm$ 1″
	ATs	$\pm$ 5″
Airy disk (FWHM	for 8 m telescopes	0.26″
at 10 μm)	for 1.8 m telescopes	1.14″
Input beam diameter	from UTs	80 mm (compressed to 18 mm)
	from ATs	18 mm
Throughput of VLTI optical train	to instrument	30 % - 35 %
Sampling time for	for fringe motion	100 ms
fringe measurement	$\leq$ 1 μm rms	
Atmospheric stability	for chopping	200 ms
Background (in Airy disk)	from sky	$2 \cdot 10^{10}$ photons/sec
	from VLTI optical train	$2 \cdot 10^{11}$ photons/sec
Detector(320 x 240 pixels)	full well capacity	$\approx 1.0 \cdot 10^{7}$ electrons
	read noise	$\leq$ 1000 electrons
Limiting N-magnitude	UTs	3 - 4 mag (1 - 2.5 Jy)
with self-fringe tracking	ATs	0 - 0.8 mag (20 - 50 Jy)
Limiting N-magnitude	UTs	8 - 9 mag (10 - 25 mJy)
with external fringe tracking*	ATs	4.8 - 5.8 mag (200 - 500 mJy)
Accuracy of visibility		$\pm$ 5 %
Phase measurement	no external referencing	differential within band
	with external referencing	possible

*Limiting magnitudes with external fringe tracking are given for an accumulated on source integration time of 1000 s, integrating over the full N band. This of course assumes that the source is bright enough at shorter wavelengths to actually perform external fringe tracking. For measurements with grism add 1 - 1.5 mag.

7. SCIENTIFIC PROGRAMME

7.1. General boundary conditions

The first requirement on a source to be observed is that fringe tracking can be performed. In the beginning this means that the source has to qualify for self-fringe tracking, i.e. to be brighter than N = 3 - 4 mag, resp. 1 - 2.5 Jy. In addition it is highly desirable that tip-tilt is possible on the source, which requires a brightness in the visual of V = 16-18 mag. Once external fringe tracking is available, the limit is set by the units involved (adaptive optics and fringe tracker) to a near-infrared brightness of about H = 9 mag (0.3 Jy) and a visual brightness of again about V = 16 mag. Large part of the source selection process therefore is dictated by source brightness. Later, the dual-beam facility PRIMA at the VLTI will allow to use neighbouring, brighter stars for fringe tracking. This will allow to go for fainter sources.

7.2. Simulation of source visibilities

The second step is to verify that the prediction leads to measurable visibilities which have the potential to answer the question leading to the observing proposal. Tools are available with ESO, the instrument teams and the interferometry centers, which typically give informations like in Figure 11 below. This particular simulation demonstrated that circumstellar disks around the components of the binary Z CMa, if at 10 μ they present an

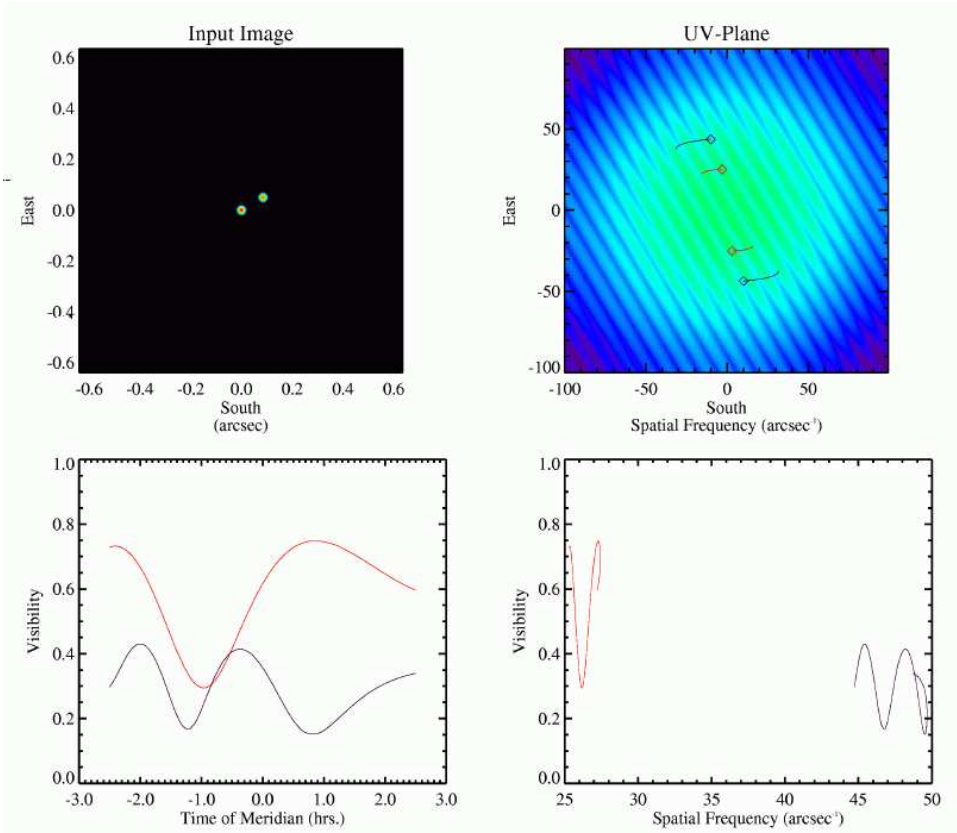

Figure 11. Simulation of an observation of the young binary Z CMa. The binary has been represented by two point sources at the actually observed separation of 0.1$''$ at P.A. 300 °, each surrounded by a circular disk with Gaussian brightness distribution and FWHM of 10 mas. From upper left to lower right we see: the image, its Fourier transform and the tracks covered by the telescope pairs UT1-UT3 (outer lines) and UT1-UT2; observed visibility as function of time and of spatial frequency. Here, the curves with the lower visibility values correspond to the baseline UT1-UT3, which will be the only one available in the beginning.

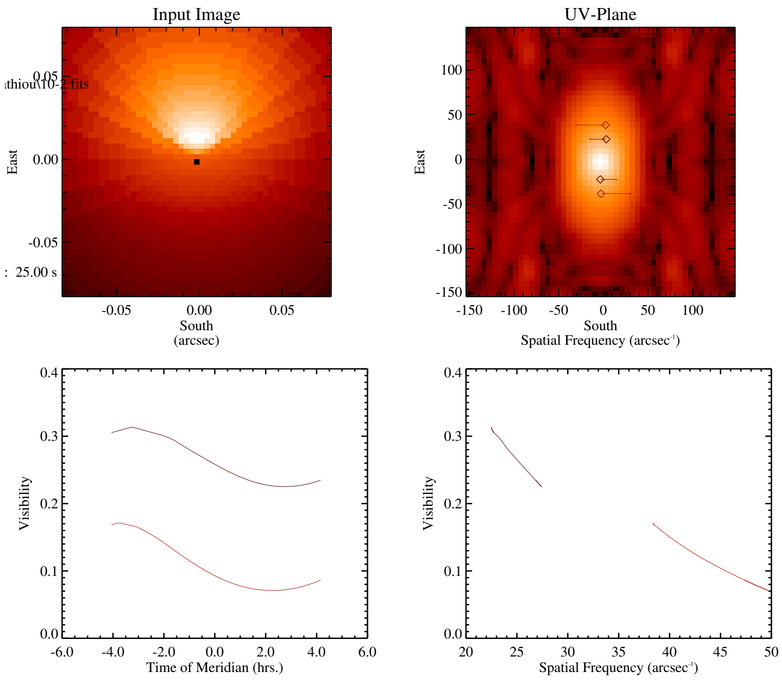

Figure 12. Same simulation, but for a model of the dusty torus in NGC 1068 seen at 65° inclination.[4]

extended emission with FWHM = 0.01″, can well be observed by the damping of the absolute visibility values with respect to those of a binary consisting of two point sources. Similarly, Figure 12 shows that the model for the dust torus of the active galactic nucleus in NGC 1068 by Efstathiou et al.[4] would lead to measurable visibilities. Here the difficulty lies in the low brightness of the objects which will make self-fringe tracking observations very difficult even for the nearest and brightest representatives of this object class.

7.3. Guaranteed time programme

Based on considerations like those described in the previous subsections we selected the following programme for execution during the 300 hours of guaranteed time available to the instrument team UTs. This listing can give an impression what may be feasible to observe with the MIDI instrument. It has to be kept in mind that the attempt for direct planet detection is a programme of extremely high risk for possibly high reward.

Topic	Telescopes	
	UTs	ATs
Dust Tori in Nearby Active Galactic Nuclei	65 h	–
Inner disks of low-mass young stellar objects	65 h	90 h
Inner disks around intermediate-mass young and Vega-type stars	62.5 h	100 h
Massive young stars	52.5 h	305 h
The dusty environment of hot stars	2 h	68 h
Cool Late Type Stars and related objects	25 h	450 h
Extra-solar planets and brown dwarfs	25 h	–

7.4. Observing on the VLTI

Actual observations on the VLTI will be performed in the same way as single-telescope observations on the VLT in general. The observations have to be composed as automatically continuing procedures in the form of so-called "observation blocks" (OBs). A description of procedures to be expected during the first two years of observations with MIDI is given by Bakker et al.[5] elsewhere in these proceedings. Underlying these procedures is the system of the MIDI software, with its ambitious task to to perform reliable operation in the VLTI environment and at the same time to provide – while self fringe tracking – the required, highly non-standard real-time synchronisation between data taking, piezo-driven OPD modulation and, if necessary, telescope chopping. A description of this largely hidden but essential part of MIDI is beyond the scope of this paper.

8. OUTLOOK

Assuming successful commissioning, MIDI on the VLTI may have first observing runs in the summer of 2003. This will be in self-fringe-tracking mode and therefore limited to brighter objects. After this the following steps are foreseen:

- Fall of 2003 – observations with additional UT baselines
  – adaptive optics and external fringe tracking, allowing to go to fainter sources
- Spring of 2004 – observations with the 1.8 m telescopes (ATs) of the auxiliary array
- Summer of 2004 – extension to 20 μm observations
  – addition of 10 μm single mode fiber in the focal plane for beam cleaning
- 2005 – introduction of dual-beam capability on the VLTI

Once these options have come to reality, MIDI should represent an instrument applicable to a wider range of astronomical studies.

ACKNOWLEDGMENTS

We thank the electronic and mechanical workshops in Heidelberg, Dwingeloo and Freiburg as well as the optical and mechanical designers for their accurate and careful work, without which the instrument would not have become reality. And we thank Sébastien Morel for many months of efficient support during the alignment and testing phase of the instrument, as well as the instrument responsibles at ESO, Markus Schoeller, Andrea Richichi and Peter Biereichel, for positively critical partnership. Markus Feldt developed the simulation tool SimVLTI, on which Figures 11 and 12 were based.

REFERENCES

1. M. Bester, W.C. Danchi, and C.H. Townes, *"Long baseline interferometer for the mid-infrared"* SPIE **1237**, 40 - 48, 1990.
2. A.W. Glazenborg-Kluttig, F. Przygodda, H. Hanenburg, S. Morel, J.-W. Pel, *"Realization of the MIDI cold optics"*, these proceedings, 2002.
3. S. Ligori, U. Graser, B. Grimm, R. Klein, *"Experiences with the Raethyon Si:As IBC detector arrays for mid-IR interferometric observations"*, these proceedings, 2002.
4. A. Efstathiou, J.H. Hough, and S. Young, *A model for the infrared continuum spectrum of NGC 1068"* MNRAS **277**, 1134 - 1144, 1995.
5. E.J. Bakker, F. Przygodda, O. Chesneau, and W. Jaffe, *"VLTI MIDI scientific observation procedures"*, these proceedings, 2002.